

# Beyond Parameter Finetuning: Test-Time Representation Refinement for Node Classification

Jiaxin Zhang

National University of Defense  
Technology  
ChangSha, Hunan, China  
zhangjiaxin18@nudt.edu.cn

Xihong Yang

Yu Shi  
Songlei Jian  
National University of Defense  
Technology  
Changsha, China

Yiqi Wang\*

National University of Defense  
Technology  
ChangSha, Hunan, China  
yiq@nudt.edu.cn

Xinwang Liu\*

National University of Defense  
Technology  
ChangSha, Hunan, China  
xinwangliu@nudt.edu.cn

Siwei Wang

Intelligent Game and Decision Lab  
Beijing, China  
wangsiwei13@nudt.edu.cn

En Zhu\*

National University of Defense  
Technology  
ChangSha, Hunan, China  
enzhu@nudt.edu.cn

## ABSTRACT

Graph Neural Networks frequently exhibit significant performance degradation in the out-of-distribution test scenario. While test-time training (TTT) offers a promising solution, existing Parameter Finetuning (PaFT) paradigm suffer from catastrophic forgetting, hindering their real-world applicability. We propose TTReFT, a novel Test-Time Representation FineTuning framework that transitions the adaptation target from model parameters to latent representations. Specifically, TTReFT achieves this through three key innovations: (1) uncertainty-guided node selection for specific interventions, (2) low-rank representation interventions that preserve pre-trained knowledge, and (3) an intervention-aware masked autoencoder that dynamically adjust masking strategy to accommodate the node selection scheme. Theoretically, we establish guarantees for TTReFT in OOD settings. Empirically, extensive experiments across five benchmark datasets demonstrate that TTReFT achieves consistent and superior performance. Our work establishes representation finetuning as a new paradigm for graph TTT, offering both theoretical grounding and immediate practical utility for real-world deployment.

## CCS CONCEPTS

• Computing methodologies → Artificial intelligence; Machine learning.

## KEYWORDS

Test Time Training, Representation Finetuning, Graph Neural Networks

\*Corresponding Author

Permission to make digital or hard copies of all or part of this work for personal or classroom use is granted without fee provided that copies are not made or distributed for profit or commercial advantage and that copies bear this notice and the full citation on the first page. Copyrights for components of this work owned by others than the author(s) must be honored. Abstracting with credit is permitted. To copy otherwise, or republish, to post on servers or to redistribute to lists, requires prior specific permission and/or a fee. Request permissions from permissions@acm.org.

Conference acronym 'XX, June 03–05, 2018, Woodstock, NY

© 2018 Copyright held by the owner/author(s). Publication rights licensed to ACM.  
ACM ISBN 978-1-4503-XXXX-X/18/06  
https://doi.org/XXXXXXX.XXXXXXX

## ACM Reference Format:

Jiaxin Zhang, Yiqi Wang, Siwei Wang, Xihong Yang, Yu Shi, Songlei Jian, Xinwang Liu, and En Zhu. 2018. Beyond Parameter Finetuning: Test-Time Representation Refinement for Node Classification. In *Proceedings of Make sure to enter the correct conference title from your rights confirmation email (Conference acronym 'XX)*. ACM, New York, NY, USA, 12 pages. <https://doi.org/XXXXXXX.XXXXXXX>

## 1 INTRODUCTION

Graph Neural Networks (GNNs) [38] are the successful extension of Deep Neural Networks (DNNs) [15] on graph data, and have achieved remarkable revolutions in graph-related applications including social network analysis [7] and recommendation systems [24, 39]. Like DNNs, most GNNs are built on the basis of the IID assumption (independent and identically distributed) between training and test data [10, 19]. However, the IID assumption is often violated in practical scenarios. Specifically, graphs can exhibit distributional shifts in either node features (attribute changes) or graph structure (homophily variations), which can lead to significant performance degradation and thus hinder practical applications.

Numerous studies have been proposed to address the aforementioned out-of-distribution (OOD) challenges [17], with prominent approaches including data augmentation to diversify training distributions [33], adversarial training for perturbation invariance [2, 37] and invariance-based causal feature learning [27]. These methods typically require multi-domain training data or rely on strong assumptions to synthesize diverse training samples that simulate unknown test features. Some even necessitate partial test data and labels for model adaptation [3]. Such requirements and assumptions are often infeasible in practice, thereby hindering their deployment. Moreover, these methods often fail to adequately explore and leverage the distributional characteristics of test data. To mitigate these issues, Test-Time Training (TTT) [28] has emerged as a novel paradigm in recent years. TTT typically employs unsupervised learning to dynamically adapt a subset of model parameters, enabling the model to better align with the distribution of test data. Multiple studies have demonstrated its effectiveness and potential in addressing OOD challenges [31, 41]. However, prevailing TTT approaches

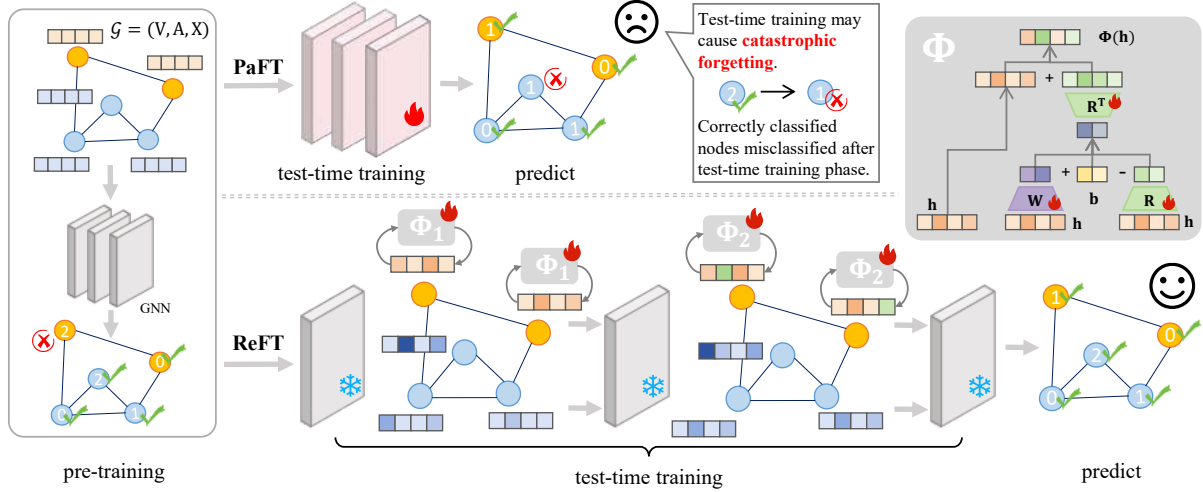


**Figure 1: A comparison of the working mechanisms of PaFT and ReFT on graphs.** (1) **Parameter Finetuning (PaFT):** The model parameters are updated during test-time training, which can lead to catastrophic forgetting, as illustrated by correctly classified training samples (blue nodes) being misclassified (turning red) after adaptation. (2) **Representation Finetuning (ReFT):** The pre-trained model parameters remain frozen. Adaptation is achieved by applying targeted, learnable interventions to a sparse subset of node representations (highlighted in yellow), successfully correcting misclassifications without forgetting pre-trained knowledge.

primarily rely on Parameter Finetuning (PaFT), a paradigm that struggles to ensure stable performance but may even induce severe problems such as catastrophic forgetting [18].

Recent advances in representation learning suggest a novel promising solution for test-time training [1, 36]. Specifically, the success of Representation Finetuning (ReFT) in Natural Language Processing (NLP) [36] demonstrates that targeted representation interventions can match full finetuning performance while modifying less than 1% of representations. Furthermore, theoretical work has established that neural networks inherently organize hierarchical semantic information within their representation spaces [4], and suggests that conventional parameter updates may disrupt these patterns. Motivated by these insights, we introduce the ReFT paradigm to the graph domain as a superior alternative to PaFT. As schematically compared in Figure 1, unlike PaFT which updates global model weights, the general ReFT paradigm keeps all pre-trained parameters frozen to prevent catastrophic forgetting. Instead, it learns targeted, low-rank interventions on hidden representations for efficient node-wise adaptation. However, seamlessly transplanting ReFT to graph data is non-trivial and faces two unique challenges: (1) Unlike NLP where interventions can target specific tokens, graph nodes are interconnected, raising the question of *which nodes should be selected for intervention?*; (2) Given the absence of test labels, *how can we guide this adaptation effectively?*

To address these challenges, we propose TTReFT, a novel Test-Time Representation FineTuning framework that instantiates ReFT for graph data as illustrated in Figure 2. To tackle the first challenge of node selection, we introduce an uncertainty-guided node selection mechanism. Instead of random selection, our approach prioritizes nodes with high predictive entropy, strategically focusing adaptation resources on uncertain samples most affected by

distribution shifts. To solve the second challenge of guidance, we design a self-supervised reconstruction task tailored for interventions. Although contrastive learning is popular [8, 23], its reliance on artificial augmentations [40] may not reflect real-world test-time shifts. Instead, we propose an intervention-aware masked autoencoder (IAMAЕ). Specifically, we align reconstruction with our adaptation objective: for each selected node, we reconstruct the features of its local neighborhood using the refined representations. This design not only encourages the refined features to fit the test distribution but also leverages local graph topology as a stability regularizer. Consequently, it generates robust self-supervision signals naturally coupled with the test-time structure, avoiding hand-crafted augmentations.

TTReFT unifies these solutions into three coordinated components as shown in Figure 2: (1) **Uncertainty-guided node selection** pinpoints high-entropy nodes as primary intervention targets; (2) **Low-rank representation intervention** applies parameter-efficient transformations solely to these selected nodes, preserving pre-trained knowledge; and (3) **Intervention-aware reconstruction** dynamically correlates masking probability with intervention density, creating a closed-loop adaptation system. Through these principled representation-space interventions, our method successfully resolves the inherent tension between adaptation and preservation. Our key contributions can be summarized as follows:

- We propose TTReFT, the first representation finetuning framework designed for graph, establishing a new paradigm for test-time training that shifts from parameter updating to representation intervention.
- We develop a novel intervention-aware masked autoencoder (IAMAЕ), which is the first to explicitly couple the masking

probability with local intervention density, enabling targeted self-supervision.

- We provide theoretical insights that demonstrate the rationality and effectiveness of representation finetuning in graph out-of-distribution (OOD) settings.
- Through extensive experiments on five datasets, we empirically validate that TTREFT consistently enhances OOD generalization while effectively preventing catastrophic forgetting of pre-trained knowledge.

## 2 PRELIMINARIES

This section defines the problem scope and contrasts two adaptation paradigms: the conventional Parameter Finetuning (PaFT) and the Representation Finetuning (ReFT).

### 2.1 Problem Formulation

We formalize the node classification task on a graph  $\mathcal{G} = (V, A, X)$ , where  $V = \{v_1, \dots, v_N\}$  denotes the node set with  $N$  nodes,  $A \in \{0, 1\}^{N \times N}$  is the adjacency matrix, and  $X \in \mathbb{R}^{N \times d}$  is the feature matrix with features dimension  $d$ .

**Graph OOD Problem.** Given a labeled source graph  $\mathcal{G}_s$  and unlabeled target graph  $\mathcal{G}_t$  with distribution shift, the goal is to adapt a pre-trained GNN  $f_\theta$  to generalize well on  $\mathcal{G}_t$ . The model parameters  $\theta$  are trained on  $\mathcal{G}_s$  via supervised loss  $L_{sup}$ .

**Graph Autoencoders (GAEs).** We employ GAEs for self-supervision. A GAE consists of an encoder  $f_E$  mapping inputs to latent representation  $\mathbf{H} \in \mathbb{R}^{N \times d_h}$ , and a decoder  $f_D$  reconstructing the graph structure or features. The reconstruction objective is generally formulated as:

$$\mathbf{H} = f_E(A, X), \quad \hat{X} = f_D(A, \mathbf{H}) \quad (1)$$

where  $\hat{X}$  denotes the reconstructed features.

### 2.2 PaFT for TTT on Graphs

Standard Test-Time Training (TTT) typically follows a Parameter Finetuning (PaFT) pipeline. Given a pre-trained  $K$ -layer GNN  $f_\theta$  with parameters  $\theta = (\theta_1, \dots, \theta_K)$ , PaFT adapts the model by:

- (1) Fixing the initial  $k$  layers  $\theta_{1:k}$  (feature extractor);
- (2) Updating remaining layers  $\theta_{k+1:K}$  by minimizing a self-supervised loss  $L_{ssl}$  on the test graph  $\mathcal{G}_t$ ;
- (3) Inferring with the updated parameters  $\theta' = (\theta_{1:k}, \theta'_{k+1:K})$ .

However, directly updating  $\theta$  often leads to catastrophic forgetting of source knowledge.

### 2.3 ReFT Paradigm on Graphs

We formalize ReFT's general application to graph TTT. Distinct from PaFT, the Representation Finetuning (ReFT) paradigm freezes all model parameters  $\theta$  and instead learns to intervene on latent representations. Let  $\mathbf{h}^{(l)}$  denote the node representations at layer  $l$ . A general ReFT intervention is defined as a tuple  $I = \langle \Phi, \mathcal{P}, \mathcal{L} \rangle$ :

- $\Phi : \mathbb{R}^d \rightarrow \mathbb{R}^d$  is a learnable intervention function parameterized by  $\phi$ .
- $\mathcal{P} \subseteq V$  is the set of target nodes to intervene.
- $\mathcal{L}$  is the set of layers where interventions are applied.

The intervened representation  $\tilde{\mathbf{h}}_v$  is computed as:

$$\tilde{\mathbf{h}}_v^{(l)} \leftarrow \mathbf{1}(v \in \mathcal{P}) \cdot \Phi(\mathbf{h}_v^{(l)}) + \mathbf{1}(v \notin \mathcal{P}) \cdot \mathbf{h}_v^{(l)} \quad (2)$$

where  $\mathbf{h}_v^{(l)}$  is the original representation of node  $v$ ,  $\tilde{\mathbf{h}}_v^{(l)}$  is the refined representation, and  $\mathbf{1}(\cdot)$  is the indicator function.

During test-time adaptation, ReFT optimizes only  $\phi$  using  $L_{ssl}$  while  $\theta$  remains frozen. This paradigm theoretically circumvents catastrophic forgetting by preserving the original model weights.

## 3 METHODOLOGY

Based on the general ReFT paradigm formalized in Section 2.3, our proposed TTREFT framework implements an efficient test-time adaptation strategy specifically tailored for graph data. By shifting the focus from parameter updates to representation interventions, TTREFT inherently circumvents catastrophic forgetting while enabling precise local adaptation.

### 3.1 Framework Overview

As illustrated in Figure 2, TTREFT freezes the pre-trained GNN  $f_\theta$  to preserve source knowledge and introduces a lightweight, plug-and-play intervention module. The adaptation process is driven by three coordinated components that instantiate the defined intervention tuple  $I = \langle \Phi, \mathcal{P}, \mathcal{L} \rangle$ : (1) **Uncertainty-Guided Node Selection** determines the target set  $\mathcal{P}$  by identifying high-entropy node; (2) **Low-Rank Representation Intervention** defines the function  $\Phi$  to apply parameter-efficient corrections to the representations of nodes in  $\mathcal{P}$ ; and (3) **Intervention-Aware Masked Autoencoders (IAMAЕ)** provides the self-supervised objective  $L_{ssl}$  to jointly optimize the intervention parameters without ground-truth labels.

### 3.2 Uncertainty-Guided Node Selection

Empirical observations (see Figure 3(b)) indicate that indiscriminate intervention among all nodes leads to both computational inefficiency and potential degradation of confident predictions. Therefore, we develop a dynamic node selection strategy that prioritizes nodes exhibiting high predictive entropy, which serves as a reliable proxy for distribution shift uncertainty.

For each test node  $v_i \in \mathcal{G}_t$ , we compute its predictive entropy as  $E_i = -\sum_{c=1}^C p(y=c \mid x_i) \log p(y=c \mid x_i)$ . This entropy measure drives a probabilistic intervention decision via a smooth thresholding mechanism:

$$p_i^{\text{intervene}} = \sigma(\alpha_{\text{gate}}(E_i - E_{\text{threshold}})), \quad (3)$$

where  $\sigma$  is the sigmoid function,  $\alpha_{\text{gate}}$  controls the sharpness of the threshold transition and  $E_{\text{threshold}}$  is a fixed threshold. The intervention mask  $\mathcal{M} \in \{0, 1\}^N$  is then sampled from a Bernoulli distribution parameterized by this probability:  $m_i^{\text{intervene}} \sim \text{Bernoulli}(p_i^{\text{intervene}})$ . The target node set is thus defined as  $\mathcal{P} = \{v_i \in \mathcal{G}_t \mid m_i^{\text{intervene}} = 1\}$ . This ensures adaptation resources are concentrated on regions where the model is least confident.

### 3.3 Low-Rank Representation Intervention

To enable efficient adaptation while preserving the essential structure of learned representations, we propose to intervene in a low-rank subspace rather than modifying the full high-dimensional

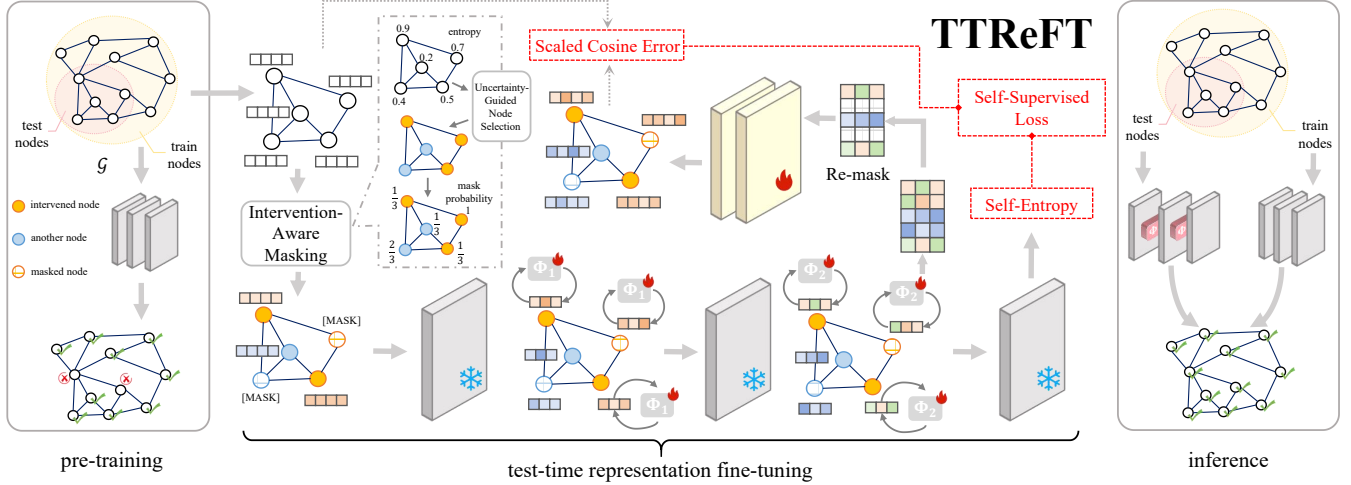


**Figure 2: The overall framework of TTReFT.** Our framework operates in three stages: (1) Pre-training: A GNN model is trained on source-domain data. All parameters are frozen after this stage. (2) Test-Time Representation Finetuning: For unlabeled test data, nodes with high predictive uncertainty (highlighted in yellow) are selected. A learnable Low-Rank Representation Intervention (LoReFT) is applied to them. The intervention parameters are optimized using a novel Intervention-Aware Masked Autoencoder (IAMAЕ) loss, which dynamically masks features based on local intervention density. (3) Inference: The frozen pre-trained model and the learned interventions are combined for final prediction, with interventions only applied to the selected uncertain nodes.

feature space. For nodes selected in the intervention set  $\mathcal{P}$ , we employ a Low-Rank Linear Representation Intervention. As shown in Figure 1, at target layer  $l \in \mathcal{L}$ , the intervention function  $\Phi^{(l)}$  transforms the original latent representation  $h_v^{(l)} \in \mathbb{R}^d$  into a refined representation:

$$\tilde{h}_v^{(l)} = h_v^{(l)} + \mathbf{R}^\top (\mathbf{W} h_v^{(l)} + \mathbf{b} - \mathbf{R} h_v^{(l)}) \quad (4)$$

where  $\mathbf{W} \in \mathbb{R}^{r \times d}$  is the low-rank projection matrix,  $\mathbf{b} \in \mathbb{R}^r$  is the bias vector, and  $\mathbf{R} \in \mathbb{R}^{r \times d}$  is the subspace basis matrix, with  $r \ll d$ . The term  $\mathbf{W}h + \mathbf{b} - \mathbf{R}h$  represents the learned modification within the  $r$ -dimensional subspace, which is then projected back to the original space via  $\mathbf{R}^\top$ . To prevent excessive deviation from the pre-trained manifold, we impose an orthogonality constraint on the rows of  $\mathbf{R}$  ( $\mathbf{R}\mathbf{R}^\top = \mathbf{I}_r$ ).

Consistent with the general ReFT definition, the intervention is applied only to the selected high-entropy nodes. The final representation used for downstream prediction is given by:

$$f_{\text{final}}(x_v) = \begin{cases} \Phi^* \circ f_\theta(x_v) & \text{if } v \in \mathcal{P}, \\ f_\theta(x_v) & \text{otherwise.} \end{cases} \quad (5)$$

where  $\Phi^*$  represents the optimal intervention function learned during test time.

This design offers three key advantages: (1) Parameter Efficiency: By optimizing only  $\{\mathbf{W}, \mathbf{b}, \mathbf{R}\}$  where  $r \ll d$ , the number of tunable parameters is reduced by orders of magnitude compared to full parameter fine-tuning. (2) Structural Preservation: The residual nature of the intervention ( $\tilde{h} = h + \Delta h$ ) ensures that the original semantic information is largely preserved, mitigating catastrophic forgetting. (3) Targeted Adaptation: By restricting updates to the

subspace defined by  $\mathbf{R}$ , we force the adaptation to focus on the most salient directions of distribution shift.

### 3.4 Intervention-Aware Masked Autoencoder

To guide the optimization of the intervention parameters  $\phi = \{\mathbf{W}, \mathbf{b}, \mathbf{R}\}$  without labeled target data, we develop an Intervention-Aware Masked Autoencoder (IAMAЕ). This approach fundamentally extends standard masked autoencoding by coupling the reconstruction task with the intervention density, recognizing that intervened nodes and their neighborhoods contain the most critical information regarding distribution shifts.

**3.4.1 Intervention-aware Masking.** Unlike standard Masked Autoencoders (MAE) that employ uniform random masking, we propose a intervention-aware adaptive masking strategy. Our intuition is that nodes surrounded by a high density of intervened neighbors are likely located in complex decision boundaries or distribution-shifted regions. These nodes should be masked with higher probability to force the model to learn more robust representations from their context.

Specifically, given the intervention mask  $\mathcal{M} \in \{0, 1\}^{|\mathcal{V}|}$ , for node  $v_i$ , we calculate its neighbor intervention count  $C_i = \sum_{v_j \in \mathcal{N}(v_i)} m_j^{\text{intervene}}$ , where  $\mathcal{N}(v_i)$  denotes the neighborhood of node  $v_i$ . The masking probability  $p_{\text{mask}}^{(i)}$  is dynamically adjusted based on its local intervention density:

$$p_{\text{mask}}^{(i)} = \rho \cdot \left( \beta + (1 - \beta) \cdot \frac{C_i}{\max_k C_k + \epsilon} \right) \quad (6)$$

where  $\rho$  is the global masking rate,  $\beta$  controls the base masking probability for nodes with no intervened neighbors, and  $\epsilon$  is a small

constant for numerical stability. This strategy systematically increases the likelihood of masking nodes in regions heavily affected by interventions, forcing the intervention module to generate features that are not only discriminative but also structurally consistent with their neighbors.

**3.4.2 Optimization Objective.** The IAMAE operates on the input graph  $\mathcal{G} = (V, A, X)$  by generating masked features  $\tilde{X}$  according to  $p_{\text{mask}}^{(i)}$ . Specifically, we sample a subset of nodes  $\tilde{V}$  to mask and replace their features with a learnable [MASK] vector. The encoder  $f_E$  corresponds to the pre-trained model  $f_\theta$  augmented with the intervention module  $\Phi$ . It takes  $\tilde{X}$  and adjacency matrix  $A$  as input to produce latent representations  $H$ . Crucially, gradients from the reconstruction loss flow through  $H$  to update the intervention parameters  $\phi$ , while  $\theta$  remains frozen.

During decoding, we apply re-masking to the representations before reconstructing the original features through a lightweight decoder  $f_D$ . This two-stage masking process ensures that the reconstruction task focuses on learning meaningful patterns from the most relevant regions of the graph. The reconstruction quality is assessed using a Scaled Cosine Error (SCE) loss:

$$L_{\text{IAMAE}} = \frac{1}{|\tilde{V}|} \sum_{v_i \in \tilde{V}} \left( 1 - \frac{x_i^\top z_i}{\|x_i\| \|z_i\|} \right)^\gamma, \quad (7)$$

where  $z_i$  is the reconstructed feature and  $\gamma \geq 1$  focuses learning on hard samples. To further regularize the adaptation, we combine this loss with self-entropy minimization [26]. While IAMAE ensures structural consistency, the entropy loss  $\mathcal{L}_e = -\sum_{c=1}^C p_c \log p_c$  promotes confident predictions by minimizing output distribution entropy. The overall self-supervised objective for test-time representation finetuning is:

$$L_{\text{ssl}} = L_{\text{IAMAE}} + \lambda_e \mathcal{L}_e \quad (8)$$

where  $\lambda_e$  is balancing coefficients.

### 3.5 Complexity Analysis

TTReFT significantly reduces computational overhead. For a graph with  $N$  nodes and feature dimension  $d$ , our method applies low-rank interventions (with rank  $r$ ) only to a selected subset of nodes  $\mathcal{P}$ . Compared to parameter finetuning which typically scales with  $\mathcal{O}(Nd^2)$  (updating full weight matrices), our method operates with  $\mathcal{O}(|\mathcal{P}|rd)$  complexity. Since  $|\mathcal{P}| \ll N$  (due to selective intervention) and  $r \ll d$  (due to low-rank design), the number of tunable parameters and floating-point operations are reduced by orders of magnitude. This ensures scalability for large-scale graph adaptation. The empirical comparisons to validate this advantage in inference time are included in Table 6.

## 4 THEORETICAL ANALYSIS

We now demonstrate the theoretical efficacy of representation intervention under distribution shifts.

**Problem Setting.** We consider a node classification task with  $C$  classes. We adopt a  $K$ -layer Simplified Graph Convolution (SGC) model [32] for its tractability while retaining graph filtering properties similar to GCNs. The model generates predictions as  $Y = \text{softmax}(A^K X W)$ , where  $W \in \mathbb{R}^{d \times C}$  is the trained weight matrix. We assume the ground-truth labels  $Y$  are generated by a 1-layer

SGC:  $Y = \text{softmax}(A X W_*)$  with a fixed underlying weight matrix  $W_* \in \mathbb{R}^{d \times C}$ .

**Algorithms.** At test time, the data undergoes a distribution shift characterized by an orthogonal transformation  $Q \in \mathbb{R}^{d \times d}$ , yielding test samples  $(\tilde{X}, Y) \sim P_t$  where  $\tilde{X} = QX$ . To mitigate this, we apply a representation intervention  $\Phi(\tilde{X}) = (1 - \alpha)\tilde{X} + \alpha UV\tilde{X}$  (simplification for LoReFT) with fixed  $U \in \mathbb{R}^{d \times m}$ ,  $V \in \mathbb{R}^{m \times d}$  ( $m \ll d$ ) and  $\alpha \in [0, 1]$ . Here,  $\alpha = 0$  corresponds to no adaptation, while  $\alpha = 1$  represents maximal intervention. Predictions use  $\hat{Y}_\alpha = \text{softmax}(A\Phi(\tilde{X})W)$ , with risk defined as:

$$\mathcal{R}(\alpha) = \mathbb{E}_{(\tilde{X}, y) \sim P_t} [\|\hat{y}_\alpha - y\|_1] \quad (9)$$

where  $\hat{y}_\alpha$  and  $y$  denote row vectors of  $\hat{Y}_\alpha$  and  $Y$ .

**Theorem 1.** *(Effectiveness of Test-Time Intervention under Orthogonal Shift).* Let  $(X, Y) \sim P$  be training samples with labels generated by  $Y = \text{softmax}(AXW)$ . Under test distribution  $P_t$  induced by  $\tilde{X} = QX$  for orthogonal  $Q$ , and given an intervention  $\Phi(\tilde{X})$  with  $U, V$  chosen to counteract  $Q$  in the prediction-relevant subspace (see Appendix), there exists  $\alpha > 0$  such that:

$$\text{Risk}(\alpha) < \text{Risk}(0). \quad (10)$$

The complete proof is detailed in Appendix D.

**Remark and Limitations.** Theorem 1 provides the first theoretical justification that representation-space intervention can strictly reduce classification risk under distribution shifts. We acknowledge that our analysis relies on simplifying assumptions to ensure mathematical tractability. However, the insight can be extended to non-linear GNNs and more complex distribution shifts, such as non-orthogonal or topological shifts, as validated by our extensive experiments on the GOOD benchmark. Extending these theoretical guarantees remains a non-trivial open problem and a promising direction for future research.

## 5 EXPERIMENT

This section presents a comprehensive evaluation of the proposed TTReFT framework. We first detail the experimental setup, then address the following research questions:

**RQ1.** Does TTReFT demonstrate superior performance in OOD generalization scenarios?

**RQ2.** How well does TTReFT maintain original task performance during adaptation?

**RQ3.** How does the self-supervised task and node selection strategy affect TTReFT's performance?

**RQ4.** How sensitive is TTReFT to its key parameters?

### 5.1 Experimental Settings

**5.1.1 Datasets.** Following the protocol of GOOD [6], we evaluate our method on five established node classification datasets: cora [20], pubmed [25], citeseer [5], wikics [21] and arxiv [12]. To evaluate OOD generalization, we design distinct data splits that explicitly separate covariate shifts (e.g., word distribution changes) from concept shifts (e.g., degree-based distribution changes). Detailed dataset statistics and splitting strategies are provided in Table 3 in Appendix A.

**Table 1: Node classification accuracy (%) on test data between TTReFT and baselines under concept\_degree split. The table is transposed to compare methods across datasets. Bold entries indicate the best performance. "OOM" means out of memory.**

| Method        | cora                               | pubmed                             | citeseer                           | wikics                             | arxiv                              |
|---------------|------------------------------------|------------------------------------|------------------------------------|------------------------------------|------------------------------------|
| EERM          | 88.44 $\pm$ 0.98                   | OOM                                | 69.30 $\pm$ 1.81                   | 79.89 $\pm$ 0.10                   | OOM                                |
| TAR           | 87.74 $\pm$ 0.23                   | 84.74 $\pm$ 0.12                   | 73.79 $\pm$ 0.22                   | 78.84 $\pm$ 0.14                   | 65.79 $\pm$ 0.17                   |
| Tent          | 87.21 $\pm$ 0.00                   | 85.09 $\pm$ 0.00                   | 70.48 $\pm$ 0.00                   | 78.63 $\pm$ 0.00                   | 65.40 $\pm$ 0.00                   |
| Gtrans        | 85.75 $\pm$ 0.02                   | 79.64 $\pm$ 0.13                   | 69.43 $\pm$ 0.23                   | 75.68 $\pm$ 0.23                   | 63.81 $\pm$ 0.21                   |
| HomoTTT       | 87.04 $\pm$ 0.00                   | 85.09 $\pm$ 0.00                   | 70.48 $\pm$ 0.00                   | 78.89 $\pm$ 0.00                   | 66.74 $\pm$ 0.00                   |
| <b>TTReFT</b> | <b>88.77 <math>\pm</math> 0.01</b> | <b>86.89 <math>\pm</math> 0.00</b> | <b>75.80 <math>\pm</math> 0.03</b> | <b>79.96 <math>\pm</math> 0.02</b> | <b>69.57 <math>\pm</math> 0.00</b> |

**Table 2: Comparison of in-distribution (ID) task performance before and after test-time training. The metric is the relative performance retention (%).**

| Dataset  | Original Accuracy (%) | Performance change (%) |        |        |         |
|----------|-----------------------|------------------------|--------|--------|---------|
|          |                       | Pre-trained Model      | TTReFT | Tent   | HomoTTT |
| cora     | 96.17                 | 0.00                   | -0.31  | -0.11  |         |
| pubmed   | 94.53                 | 0.00                   | -0.41  | -0.13  |         |
| citeseer | 99.34                 | 0.00                   | -21.13 | -25.32 |         |
| wikics   | 86.84                 | 0.00                   | -0.71  | -0.51  |         |

**5.1.2 Evaluation and Implementation.** We adopt the widely used metric accuracy to evaluate the model performance. All experiments were conducted five times using different seeds and the mean performance is reported. The pipeline can be applied to any GNN model, with the most popular GCN [14] being adopted in this experiment. The results of other GNN model (GAT [29] and SAGE [7]) are detailed in Appendix. Instead of undergoing complex tuning, we fixed the learning rate used in prior studies for all datasets. The code and more implementation details are available in supplementary material.

**5.1.3 Baselines.** We compare TTReFT against state-of-the-art approaches categorized into two groups: Graph-specific Domain Generalization (DG) and Test-Time Training. The DG group includes (1) EERM [35], which employs environment-based regularization, and (2) TAR [43], a recent SOTA method utilizing topology-aware dynamic reweighting strategies. The TTT group comprises (3) Tent [30], a general entropy minimization approach adapted from vision; (4) GTrans [13], a graph transformation method; and (5) HomoTTT [42], an SSL-based fully TTT framework. For fair comparison, all methods are allocated the same tuning budget. Note that EERM triggered out-of-memory (OOM) errors on pubmed and arxiv using a 24GB NVIDIA 4090 GPU.

## 5.2 OOD Generalization Performance (RQ1)

To evaluate TTReFT’s effectiveness in OOD scenarios, we conduct a comprehensive comparison with five state-of-the-art OOD generalization methods. The accuracy results are summarized in

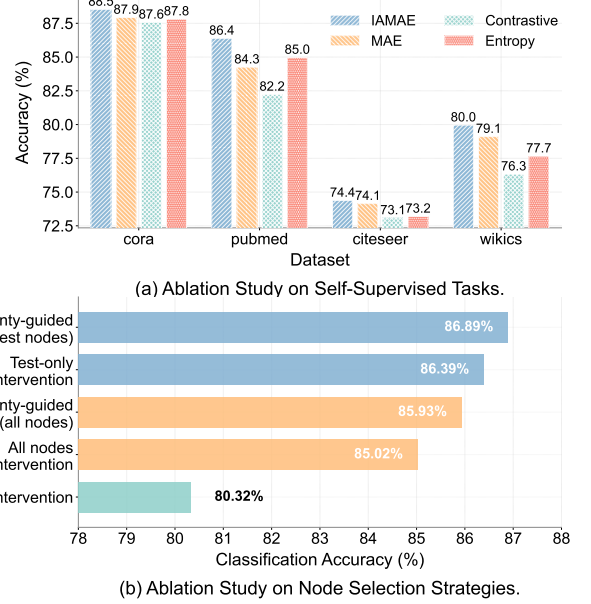


**Figure 3: Ablation studies on key components.** (a) Comparison of different self-supervised objectives for guiding intervention optimization. (b) Impact of node selection strategies on pubmed dataset. The bars represent accuracy when applying interventions to: no nodes (baseline), all nodes, test nodes, and our uncertainty-guided subset (top 10% entropy).

Table 1, revealing three key findings: (1) TTReFT consistently outperforms parameter finetuning methods across all datasets. This demonstrates that targeted adjustments to minimal node representations can effectively compensate for distribution shifts without the need for full parameter optimization. (2) While EERM outperforms others in most scenarios, its computational overhead limits practical deployment. This contrast highlights the advantage of post-hoc methods like TTReFT that maintain plug-and-play simplicity without requiring expensive retraining of pre-trained models. (3) Robustness on Large-Scale Graphs: On the largest dataset, TTReFT achieves improvement over the strong baseline TAR, proving its scalability and robustness in handling complex, real-world distribution shifts.

## 5.3 Catastrophic Forgetting Analysis (RQ2)

We quantitatively evaluate catastrophic forgetting by measuring the performance change on in-distribution (ID) data after test-time training. As shown in Table 2, our framework preserves 100% of its original accuracy. This is structurally guaranteed by our design, which freezes the pre-trained parameters and confines adaptation to the representation space. In sharp contrast, parameter finetuning baselines suffer significant degradation due to catastrophic forgetting, rendering the adapted models unusable for the original task.

## 5.4 Ablation Study (RQ3)

We validate two key components of TTReFT: the Intervention-Aware Masked Autoencoder and the Uncertainty-Guided Node

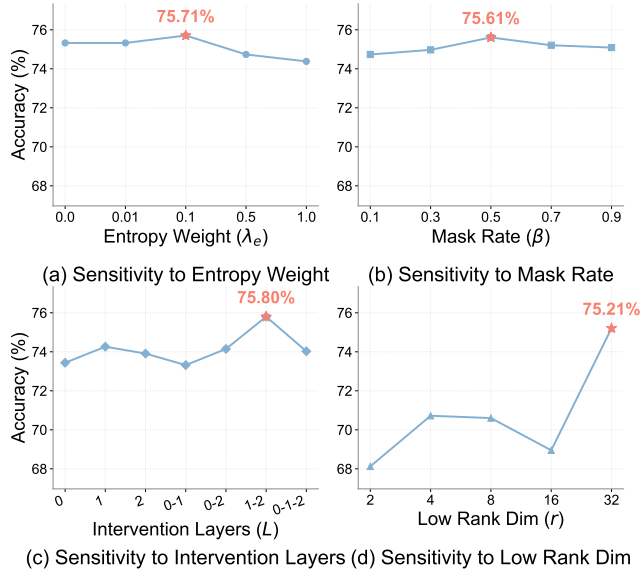


**Figure 4: Sensitivity analysis of hyperparameters on the citeseer dataset. The ★ marks the optimal value for each parameter.**

Selection. Firstly, we compare IMAAE against three baselines: standard MAE, Contrastive learning, and Entropy minimization. As shown in Figure 3(a), IMAAE consistently outperforms all variants across four datasets. This superiority stems from its dynamic masking strategy, which forces the model to reconstruct structurally significant features in high-intervention regions rather than learning trivial patterns. Then, we evaluate different selection strategies on pubmed in Figure 3(b). Our Uncertainty-Guided approach achieves the highest accuracy, significantly surpassing Random Selection and No Intervention. Notably, intervening on Test-only nodes yields better results than All nodes, suggesting that adapting training nodes introduces unnecessary noise (over-adaptation). These results confirm that prioritizing uncertain test nodes effectively targets samples most affected by distribution shifts.

### 5.5 Sensitivity Analysis (RQ4)

We examine the impact of four hyperparameters on citeseer, as shown in Figure 4. (1) **Robustness of entropy weight ( $\lambda_e$ ) and mask rate ( $\beta$ ).** The model exhibits high robustness to both the  $\lambda_e$  and  $\beta$ . Performance remains stable for  $\lambda_e \in [0.0, 0.1]$  and  $\beta \in [0.1, 0.9]$ , peaking at  $\lambda_e = 0.1$  and  $\beta = 0.5$ . Excessive entropy weight degrades performance by inducing over-confidence, while extreme mask rates disrupt the balance between self-supervision signals and structural context preservation. (2) **Intervention Layers.** Our results confirm that intervening on deeper layers significantly outperforms shallow ones, with multi-layer intervention yielding the best accuracy. Generally, deeper pre-trained backbones require interventions across more layers to effectively correct shifted representations as shown in Table 7 in Appendix. (3) **Low-Rank Dimension.** The optimal rank  $r$  varies significantly across datasets, reflecting the complexity of the required adaptation. On citeseer, performance

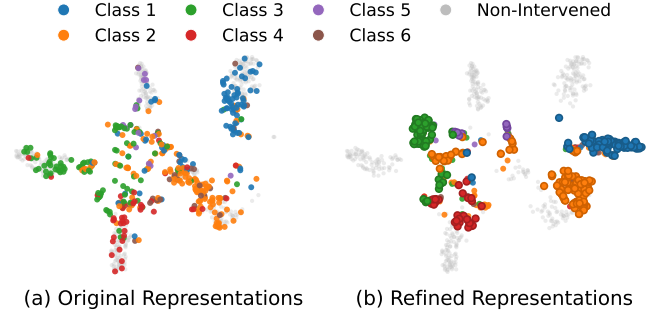


**Figure 5: Visualization of representation refinement using t-SNE.**

improves as  $r$  increases, indicating that a higher-capacity intervention is needed to correct significant distribution shifts. Conversely, for datasets like cora and pubmed (detailed in Appendix), a minimal rank ( $r = 4$ ) is sufficient. This suggests that  $r$  should be tuned to balance the expressiveness required for adaptation against the risk of overfitting, rather than simply maximizing the rank.

## 5.6 Visualization

To verify the efficacy of TTREFT, we visualize citeseer node representations before and after adaptation in Figure 5. Initially, nodes subject to distribution shift (colored) exhibit considerable overlap across class boundaries, leading to misclassification. After adaptation, these nodes significantly shift towards their ground-truth clusters, forming compact and distinct boundaries. This confirms that our representation finetuning effectively corrects shifted features by realigning them with the in-distribution manifold, directly improving classification accuracy.

## 6 RELATED WORK

The related works of TTREFT are discussed as follows:

### 6.1 Graph OOD Generalization

Graph OOD generalization aims to learn GNNs robust to distribution shifts. Invariant Learning approaches seek to capture stable substructures across environments. EERM [35] and OOD-GNN [16] minimize risk variance or remove spurious correlations to achieve invariance. SR-GNN [44] employs adversarial clustering to enforce class separation under shifts. Augmentation methods enhance robustness by diversifying training data. GSAT [22] extracts robust subgraphs by filtering environmental bias, while TAR [43] uses topology-aware reweighting to handle structural shifts. While effective, these methods heavily rely on diverse training domains or strong assumptions to simulate OOD patterns during training. In contrast, TTREFT adopts a test-time training paradigm, enabling on-the-fly adaptation to unknown shifts without revisiting source data.

### 6.2 Test-Time Training on Graphs

Test-time training [28] has emerged as a promising paradigm for addressing out-of-distribution (OOD) challenges. GT3 [31] pioneered

TTT for graph neural networks via contrastive learning. Subsequent approaches introduce node-level adaptations: HomOTT leverages homophily priors [42], while LLMTTT incorporates language model annotations [41]. However, these methods fundamentally suffer from catastrophic forgetting due to gradient conflicts [18]. Our work circumvents these issues through a novel representation-space adaptation paradigm.

### 6.3 Representation Finetuning

Representation finetuning shifts the adaptation paradigm from adjusting model parameters to directly intervening on hidden representations. Pioneered by ReFT [36], which shows that such interventions can match or exceed full finetuning performance, this approach is further advanced by RED [34] via targeted network edits for high parameter efficiency. By completely decoupling adaptation from parameter updates, these methods effectively preserve pre-trained knowledge. However, existing techniques are graph-agnostic. Our work is the first to systematically introduce the representation fine-tuning paradigm into the graph domain

## 7 CONCLUSION

This paper presents TTREFT, a novel test-time representation finetuning framework designed to circumvent the persistent challenge of catastrophic forgetting in test-time training (TTT). By shifting the adaptation paradigm from direct parameter updates to targeted representation interventions, TTREFT achieves robust out-of-distribution generalization while strictly preserving pre-trained knowledge. We establish a principled methodology for graph TTT, characterized by an uncertainty-guided node selection strategy and an intervention-aware masked reconstruction objective. As a light-weight, modular component, TTREFT seamlessly integrates with existing architectures without necessitating structural modifications. Both extensive empirical evaluations across diverse benchmarks and theoretical analysis confirm the efficacy of this representation-centric approach. Beyond advancing TTT techniques for graph data, our work paves the way for future research into dynamic graph adaptation and scalable deep learning through the lens of principled representation refinement.

## ACKNOWLEDGMENTS

To Robert, for the bagels and explaining CMYK and color spaces.

## REFERENCES

- [1] Angelica Chen, Ravid Shwartz-Ziv, Kyunghyun Cho, Matthew L Leavitt, and Naomi Saphra. 2023. Sudden drops in the loss: Syntax acquisition, phase transitions, and simplicity bias in MLMs. *arXiv preprint arXiv:2309.07311* (2023).
- [2] Fuli Feng, Xiangnan He, Jie Tang, and Tat-Seng Chua. 2019. Graph adversarial training: Dynamically regularizing based on graph structure. *IEEE Transactions on Knowledge and Data Engineering* 33, 6 (2019), 2493–2504.
- [3] Wenzheng Feng, Jie Zhang, Yuxiao Dong, Yu Han, Huanbo Luan, Qian Xu, Qiang Yang, Evgeny Kharlamov, and Jie Tang. 2020. Graph random neural networks for semi-supervised learning on graphs. *Advances in neural information processing systems* 33 (2020), 22092–22103.
- [4] Atticus Geiger, Hanson Lu, Thomas Icard, and Christopher Potts. 2021. Causal abstractions of neural networks. *Advances in Neural Information Processing Systems* 34 (2021), 9574–9586.
- [5] C. Lee Giles, Kurt D. Bollacker, and Steve Lawrence. 1998. CiteSeer: an automatic citation indexing system. In *Proceedings of the Third ACM Conference on Digital Libraries* (Pittsburgh, Pennsylvania, USA) (DL '98). Association for Computing Machinery, New York, NY, USA, 89–98. <https://doi.org/10.1145/276675.276685>
- [6] Shurui Gui, Xiner Li, Limei Wang, and Shuiwang Ji. 2022. GOOD: A Graph Out-of-Distribution Benchmark. *arXiv:2206.08452* [cs.LG]
- [7] Will Hamilton, Zhitao Ying, and Jure Leskovec. 2017. Inductive representation learning on large graphs. *Advances in neural information processing systems* 30 (2017).
- [8] Kaveh Hassani and Amir Hosein Khasahmadi. 2020. Contrastive multi-view representation learning on graphs. In *International conference on machine learning*. PMLR, 4116–4126.
- [9] Kaiming He, Xinlei Chen, Saining Xie, Yanghao Li, Piotr Dollár, and Ross Girshick. 2022. Masked autoencoders are scalable vision learners. In *Proceedings of the IEEE/CVF conference on computer vision and pattern recognition*. 16000–16009.
- [10] Dan Hendrycks and Thomas Dietterich. 2019. Benchmarking neural network robustness to common corruptions and perturbations. *arXiv preprint arXiv:1903.12261* (2019).
- [11] Edward J Hu, Yelong Shen, Phillip Wallis, Zeyuan Allen-Zhu, Yuanzhi Li, Shean Wang, Lu Wang, Weizhu Chen, et al. 2022. Lora: Low-rank adaptation of large language models. *ICLR* 1, 2 (2022), 3.
- [12] Weihua Hu, Matthias Fey, Marinka Zitnik, Yuxiao Dong, Hongyu Ren, Bowen Liu, Michele Catasta, and Jure Leskovec. 2021. Open Graph Benchmark: Datasets for Machine Learning on Graphs. *arXiv:2005.00687* [cs.LG]
- [13] Wei Jin, Tong Zhao, Jiayuan Ding, Yozhen Liu, Jiliang Tang, and Neil Shah. 2022. Empowering graph representation learning with test-time graph transformation. *arXiv preprint arXiv:2210.03561* (2022).
- [14] Thomas N. Kipf and Max Welling. 2017. Semi-Supervised Classification with Graph Convolutional Networks. *arXiv:1609.02907* [cs.LG]
- [15] Yann LeCun, Yoshua Bengio, and Geoffrey Hinton. 2015. Deep learning. *nature* 521, 7553 (2015), 436–444.
- [16] Haoyang Li, Xin Wang, Ziwei Zhang, and Wenwu Zhu. 2022. Ood-gnn: Out-of-distribution generalized graph neural network. *IEEE Transactions on Knowledge and Data Engineering* 35, 7 (2022), 7328–7340.
- [17] Haoyang Li, Xin Wang, Ziwei Zhang, and Wenwu Zhu. 2022. Out-of-distribution generalization on graphs: A survey. *arXiv preprint arXiv:2202.07987* (2022).
- [18] Yuejiang Liu, Parth Kothari, Bastien Van Delft, Baptiste Bellot-Gurlet, Taylor Mordam, and Alexandre Alahi. 2021. Ttt++: When does self-supervised test-time training fail or thrive? *Advances in Neural Information Processing Systems* 34 (2021), 21808–21820.
- [19] Massimiliano Mancini, Zeynep Akata, Elisa Ricci, and Barbara Caputo. 2020. Towards recognizing unseen categories in unseen domains. In *European Conference on Computer Vision*. Springer, 466–483.
- [20] Andrew Kachites McCallum, Kamal Nigam, Jason Rennie, and Kristie Seymore. 2000. Automating the construction of internet portals with machine learning. *Information Retrieval* 3, 2 (2000), 127–163.
- [21] Péter Mernyei and Cătălina Cangea. 2022. Wiki-CS: A Wikipedia-Based Benchmark for Graph Neural Networks. *arXiv:2007.02901* [cs.LG]
- [22] Siqi Miao, Mia Liu, and Pan Li. 2022. Interpretable and generalizable graph learning via stochastic attention mechanism. In *International conference on machine learning*. PMLR, 15524–15543.
- [23] Jiezhang Qiu, Qibin Chen, Yuxiao Dong, Jing Zhang, Hongxia Yang, Ming Ding, Kuansan Wang, and Jie Tang. 2020. Gcc: Graph contrastive coding for graph neural network pre-training. In *Proceedings of the 26th ACM SIGKDD international conference on knowledge discovery & data mining*. 1150–1160.
- [24] Andrea Rossi, Denilson Barbosa, Donatella Firmani, Antonio Matinata, and Paolo Merialdo. 2021. Knowledge graph embedding for link prediction: A comparative analysis. *ACM Transactions on Knowledge Discovery from Data (TKDD)* 15, 2 (2021), 1–49.
- [25] Prithviraj Sen, Galileo Namata, Mustafa Bilgic, Lise Getoor, Brian Gallagher, and Tina Eliassi-Rad. 2008. Collective classification in network data. *AI magazine* 29, 3 (2008), 93–93.
- [26] Claude E Shannon. 1948. A mathematical theory of communication. *The Bell system technical journal* 27, 3 (1948), 379–423.
- [27] Yu Song and Donglin Wang. 2022. Learning on graphs with out-of-distribution nodes. In *Proceedings of the 28th ACM SIGKDD Conference on Knowledge Discovery and Data Mining*. 1635–1645.
- [28] Yu Sun, Xiaolong Wang, Zhuang Liu, John Miller, Alexei Efros, and Moritz Hardt. 2020. Test-time training with self-supervision for generalization under distribution shifts. In *International conference on machine learning*. PMLR, 9229–9248.
- [29] Petar Veličković, Guillem Cucurull, Arantxa Casanova, Adriana Romero, Pietro Lio, and Yoshua Bengio. 2017. Graph attention networks. *arXiv preprint arXiv:1710.10903* (2017).
- [30] Dequan Wang, Evan Shelhamer, Shaoteng Liu, Bruno Olshausen, and Trevor Darrell. 2020. Tent: Fully test-time adaptation by entropy minimization. *arXiv preprint arXiv:2006.10726* (2020).
- [31] Yiqi Wang, Chaozhuo Li, Wei Jin, Rui Li, Jianan Zhao, Jiliang Tang, and Xing Xie. 2022. Test-time training for graph neural networks. *arXiv preprint arXiv:2210.08813* (2022).
- [32] Felix Wu, Amauri Souza, Tianyi Zhang, Christopher Fifty, Tao Yu, and Kilian Weinberger. 2019. Simplifying graph convolutional networks. In *International*

conference on machine learning. Pmlr, 6861–6871.

[33] Lirong Wu, Haitao Lin, Yufei Huang, and Stan Z Li. 2022. Knowledge distillation improves graph structure augmentation for graph neural networks. *Advances in Neural Information Processing Systems* 35 (2022), 11815–11827.

[34] Muling Wu, Wenhao Liu, Xiaohua Wang, Tianlong Li, Changze Lv, Zixuan Ling, Jianhao Zhu, Cenyuan Zhang, Xiaoqing Zheng, and Xuanjing Huang. 2024. Advancing parameter efficiency in fine-tuning via representation editing. *arXiv preprint arXiv:2402.15179* (2024).

[35] Qitian Wu, Hengrui Zhang, Junchi Yan, and David Wipf. 2022. Handling distribution shifts on graphs: An invariance perspective. *arXiv preprint arXiv:2202.02466* (2022).

[36] Zhengxuan Wu, Aryaman Arora, Zheng Wang, Atticus Geiger, Dan Jurafsky, Christopher D Manning, and Christopher Potts. 2024. Reft: Representation finetuning for language models. *Advances in Neural Information Processing Systems* 37 (2024), 63908–63962.

[37] Kaidi Xu, Hongge Chen, Sijia Liu, Pin-Yu Chen, Tsui-Wei Weng, Mingyi Hong, and Xue Lin. 2019. Topology attack and defense for graph neural networks: An optimization perspective. *arXiv preprint arXiv:1906.04214* (2019).

[38] Keyulu Xu, Weihua Hu, Jure Leskovec, and Stefanie Jegelka. 2018. How powerful are graph neural networks? *arXiv preprint arXiv:1810.00826* (2018).

[39] Xihong Yang, Yiqi Wang, Jin Chen, Wenqi Fan, Xiangyu Zhao, En Zhu, Xinxing Liu, and Defu Lian. 2025. Dual test-time training for out-of-distribution recommender system. *IEEE Transactions on Knowledge and Data Engineering* (2025).

[40] Hengrui Zhang, Qitian Wu, Junchi Yan, David Wipf, and Philip S Yu. 2021. From canonical correlation analysis to self-supervised graph neural networks. *Advances in Neural Information Processing Systems* 34 (2021), 76–89.

[41] Jiaxin Zhang, Yiqi Wang, Xihong Yang, Siwei Wang, Yu Feng, Yu Shi, Ruichao Ren, En Zhu, and Xinxing Liu. 2024. Test-time training on graphs with large language models (llms). In *Proceedings of the 32nd ACM International Conference on Multimedia*. 2089–2098.

[42] Jiaxin Zhang, Yiqi Wang, Xihong Yang, and En Zhu. 2024. A fully test-time training framework for semi-supervised node classification on out-of-distribution graphs. *ACM Transactions on Knowledge Discovery from Data* 18, 7 (2024), 1–19.

[43] Weihuang Zheng, Jiahu Liu, Jiaxing Li, Jiayun Wu, Peng Cui, and Youyong Kong. 2025. Topology-Aware Dynamic Reweighting for Distribution Shifts on Graph. In *Forty-second International Conference on Machine Learning*.

[44] Qi Zhu, Chao Zhang, Chanyoung Park, Carl Yang, and Jiawei Han. 2022. Shift-robust node classification via graph adversarial clustering. *arXiv preprint arXiv:2203.15802* (2022).

**Table 3: The description of datasets. A summary of the key statistics for the node classification datasets used in our experiments, including the number of classes, nodes, edges, and test nodes. The datasets are partitioned using the GOOD benchmark to explicitly create out-of-distribution splits based on criteria like node degree and feature (word).**

| Dataset  | Class | Nodes  | Edges   | Test nodes |
|----------|-------|--------|---------|------------|
| cora     | 7     | 2708   | 5429    | 837        |
| pubmed   | 3     | 19717  | 44338   | 6001       |
| citeseer | 6     | 3186   | 4732    | 847        |
| wikics   | 10    | 11701  | 216123  | 3308       |
| arxiv    | 40    | 169343 | 1166243 | 51480      |

## A DATASETS

This paper utilizes popular datasets commonly used for node classification tasks, namely cora [20], pubmed [25], citeseer [5], arxiv [12], and wikics [21]. Afterwards, we apply the GOOD [6] split method to partition the aforementioned datasets. GOOD make distinctions between concept shifts and covariate shifts. We select degree and word (time in arxiv) as the criteria for domain division. According to different split methods, we generated four out-of-distribution (OOD) datasets for each dataset.

## B FURTHER EXPERIMENTAL STUDIES

### B.1 Ablation on the Decoder Architecture

**Table 4: The ablation of the decoder architecture. Node classification accuracy (%) for TTReFT using different decoder architectures in the IMAAE module. The GCN-based decoder, which leverages graph structural information for feature reconstruction, consistently yields the best performance, validating its design for graph-structured data.**

| Dataset  | GCN_based    | MLP_based | Linear_based |
|----------|--------------|-----------|--------------|
| cora     | <b>88.77</b> | 87.81     | 88.05        |
| pubmed   | <b>86.89</b> | 84.15     | 85.78        |
| citeseer | <b>75.80</b> | 74.69     | 74.80        |
| wikics   | <b>79.96</b> | 76.75     | 76.15        |

The decoder  $f_D$  maps the latent code  $H$  back to the input  $X$ , and its design would depend on the semantic level [9] of target  $X$ . In graphs, the decoder reconstructs relatively less informative multi-dimensional node features. In our proposed TTReFT, IMAAE uses GCN [14] as the decoder. To have a fair comparison and investigate the influence of the backbone of decoder, we compare the results of different datasets using GCN, MLP and Linear as the decoder. The results are shown in Table 4. It demonstrates that with the GNN decoder, a masked node is forced to reconstruct its input feature from the neighboring unmasked latent representations.

**Table 5: The ablation on the representation intervention instances. Performance comparison of different intervention mechanisms: our proposed LoReFT, a simplified variant without orthogonality constraints (DiReFT), and a minimal baseline using UV-decomposition (UV). The results demonstrate the importance of the orthogonal projection and residual design in LoReFT for effective and stable representation adaptation.**

| Dataset  | LoReFT       | DiReFT | UV    |
|----------|--------------|--------|-------|
| cora     | <b>88.77</b> | 87.14  | 88.03 |
| pubmed   | <b>86.89</b> | 83.67  | 83.34 |
| citeseer | <b>75.80</b> | 74.48  | 74.31 |
| wikics   | <b>79.96</b> | 76.94  | 77.32 |

## B.2 Ablation on the Representation Intervention Instance

To investigate the impact of intervention mechanisms on model representation finetuning, we conduct ablation studies centered on the low-rank linear subspace finetuning method LoReFT. Three comparative variants are constructed:

**Baseline Method (LoReFT):** Following the original formulation, LoReFT intervenes hidden representations within an  $r$ -dimensional subspace spanned by the row vectors of matrix  $R$  through the projection source  $\mathbf{R}s = \mathbf{W}\mathbf{h} + \mathbf{b}$ . Parameters  $\{\mathbf{R}, \mathbf{W}, \mathbf{b}\}$  are learnable while the pre-trained model remains frozen. Critically,  $\mathbf{R} \in \mathbb{R}^{r \times d}$  is enforced as row-orthogonal to ensure subspace regularity and mitigate representation collapse.

**Simplified Variant (DiReFT):** We remove LoReFT’s orthogonality constraint and residual mechanism, reducing it to  $\Phi_{\text{DiReFT}}(\mathbf{h}) = \mathbf{h} + \mathbf{W}_2^\top (\mathbf{W}_1 \mathbf{h} + \mathbf{b})$ . Here,  $\mathbf{W}_1, \mathbf{W}_2 \in \mathbb{R}^{r \times d}$  are unconstrained low-rank projection matrices. This variant reduces computational overhead and aligns with direct hidden-state interventions like LoRA [11].

**Control Method (UV-Decomposition):** As a minimal-intervention baseline, we introduce elementary low-rank matrix factorization:  $\Phi_{\text{UV}}(\mathbf{h}) = \mathbf{h} + \mathbf{U}\mathbf{V}^\top \mathbf{h}$ , where  $\mathbf{U}, \mathbf{V} \in \mathbb{R}^{d \times r}$ . This approach applies no subspace constraints or nonlinear projections.

This ablation isolates the effects of (i) orthogonality constraints, (ii) residual design, and (iii) projection complexity on low-rank adaptation efficacy. Table 5 shows the effectiveness of our intervention mechanisms.

## B.3 Efficiency Comparison

Beyond its strong out-of-distribution generalization performance, the proposed TTReFT framework achieves a significant improvement in test-time efficiency compared to traditional parameter finetuning (PaFT) methods. As shown in Table 6, efficiency metrics are measured on the PubMed dataset during the test-time training phase. A higher Avg. Time indicates faster adaptation. The number of tunable parameters for TTReFT is determined by the low-rank dimension  $r$  and representation dimension  $d$ , which is independent of the model size. TTReFT requires substantially less computation time and memory during the test-time adaptation phase, thanks to its parameter-efficient representation intervention strategy.

While PaFT methods must compute gradients and update a large portion of the model’s parameters, TTReFT only optimizes a small set of low-rank intervention matrices while keeping all pre-trained parameters frozen. This approach reduces the number of tunable parameters by orders of magnitude—from  $O(Nd^2)$  to  $O(|P|rd)$ —resulting in faster convergence and lower memory footprint. The efficiency gains are particularly pronounced on larger graphs, where TTReFT maintains stable memory usage while PaFT baselines often encounter out-of-memory (OOM) errors. These advantages make TTReFT highly practical for real-world deployment where test-time computational resources are often limited.

## C IMPLEMENTATION DETAILS

### C.1 Environment

All experiments (including main experiments and comparison experiments) are conducted on Windows servers equipped with an NVIDIA 4090 GPU. Models are implemented in PyTorch version 2.1.0 with CUDA version 12.1, scikit-learn version 1.3.2 and Python 3.8.

### C.2 Model Configuration

For node classification, we train the model using Adam Optimizer with  $\beta_1 = 0.9, \beta_2 = 0.999, \varepsilon = 110 - 8$ . More details about hyperparameters and datasets are in Table 7. The intervention layers  $L$  can be either a single layer or any set of consecutive layers from the pre-trained GNN model, allowing flexible adaptation at different semantic levels.

## D FURTHER THEORETICAL ANALYSIS

Let  $x, y \sim P$  denote the training distribution. Consider a node classification task with  $C$  classes using a  $K$ -layer Simplified Graph Convolution (SGC) [32] model. The node representation is given by  $Z = A^K X W$ , where  $A$  is the adjacency matrix,  $X$  is the feature matrix, and  $W \in \mathbb{R}^{n \times d}$  is the weight matrix. Assume the ground-truth label  $y$  is generated as  $y = \text{softmax}(AxW)$  with  $K = 1$ .

At test time, we simulate distribution shift in the test samples using an orthogonal transformation  $Q$ , and we observe shifted samples  $(\tilde{x}, y) \sim P_t$  with  $\tilde{x} = Qx$ . We then apply a test-time intervention  $\Phi(\tilde{x}) = (1 - \alpha)\tilde{x} + \alpha UV\tilde{x}$ , where  $\alpha$  is a hyper-parameter, and predict  $\hat{y}_\alpha = \text{softmax}(A\Phi(\tilde{x})W)$ . Define the prediction risk as  $\text{Risk}(\alpha) = \mathbb{E}[\|\hat{y}_\alpha - y\|_1]$ , where the expectation is taken over  $P_t$ .

To facilitate the subsequent proof, we state the following assumptions:

- (1) The intervention operation is effective, i.e.,  $\mathbb{E}[\|(UVQ - I)x\|_2^2] < \mathbb{E}[\|(Q-I)x\|_2^2]$ . This indicates that the intervention effect after processing with  $UV$  is superior to that without  $UV$  processing.
- (2) The training feature  $x$  is bounded, satisfying  $\|x\|_2 \leq M$  almost surely. Its expectation is zero ( $\mathbb{E}[x] = 0$ ) and its covariance matrix is  $\Sigma_x$  ( $\text{Cov}(x) = \Sigma_x$ ).
- (3) The softmax function satisfies Lipschitz continuity, i.e., there exists a constant  $L > 0$  such that  $\|\text{softmax}(z) - \text{softmax}(z')\|_1 \leq L\|z - z'\|_2$ . This implies that the  $\ell_1$ -norm difference of the softmax output is controlled by the  $\ell_2$ -norm difference of the input with a coefficient  $L$ .

**Table 6: Empirical efficiency comparison of test-time adaptation methods. Metrics were measured on the PubMed dataset. TTReFT achieves a superior trade-off by optimizing a minimal set of low-rank parameters.**

| Method               | Adaptation Type                    | Avg. Time (s) ↓ | Peak Memory (GB) ↓ | Tunable Parameters               |
|----------------------|------------------------------------|-----------------|--------------------|----------------------------------|
| EERM                 | Environment Inference              | OOM             | >24                | $O(\#environments)$              |
| Tent                 | Parameter Modulation               | 28.4            | 6.5                | $\gamma, \beta \in \mathbb{R}^d$ |
| HomoTTT              | Full Parameter Finetuning          | 35.1            | 7.2                | $\sim 100\% \text{ of } \theta$  |
| <b>TTReFT (Ours)</b> | <b>Representation Intervention</b> | <b>5.8</b>      | <b>2.1</b>         | <b>R, W, b</b>                   |

**Table 7: Hyperparameter configurations of the proposed TTReFT framework across different datasets. The table presents the optimal values found for each key parameter during validation, along with their respective tuning ranges.**

| Hyperparameter      | Symbol                 | Optimal Value by Dataset |        |          |        | Search Space | Description          |
|---------------------|------------------------|--------------------------|--------|----------|--------|--------------|----------------------|
|                     |                        | cora                     | pubmed | citeseer | wikics | arxiv        |                      |
| Low-rank dimension  | $r$                    | 8                        | 32     | 32       | 4      | 2            | {2, 4, 8, 16, 32}    |
| Intervention layers | $L$                    | 1                        | [1, 2] | [2, 3]   | 2      | 1            | {1, 2, ..., K}       |
| Learning rate       | $\eta$                 | 0.01                     | 0.01   | 0.0003   | 0.008  | 0.006        | $[10^{-4}, 10^{-2}]$ |
| Entropy loss weight | $\lambda_e$            | 0.1                      | 0.1    | 0.1      | 0.1    | 0.1          | fixed                |
| Gate temperature    | $\alpha_{\text{gate}}$ | 10                       | 10     | 10       | 10     | 10           | fixed                |
| Global mask rate    | $\rho$                 | 0.7                      | 0.2    | 0.5      | 0.3    | 0.2          | [0, 0.8]             |
| Base mask rate      | $\beta$                | 0.5                      | 0.5    | 0.5      | 0.5    | 0.5          | fixed                |

(4) The test distribution  $P_t$  is the distribution of  $(QX, Y)$  where  $(X, Y) \sim P$ .

Under these assumptions, there exists  $\alpha > 0$  such that  $Risk(\alpha) < Risk(0)$ .

**Proof.** We establish the theorem by demonstrating that the test-time intervention reduces the expected deviation between the true logits and the predicted logits, which subsequently lowers the prediction risk due to the Lipschitz continuity of the softmax function. The proof proceeds through five interconnected stages.

### 1. Logit Formulation and Residual Analysis

Let  $x$  denote the feature vector of a test node. The ground-truth logits are given by:

$$z_{\text{true}} = AxW. \quad (1)$$

Under test-time distribution shift, we observe  $\tilde{x} = Qx$ , where  $Q$  is an orthogonal matrix. The test-time intervention transforms the shifted features as:

$$\Phi(\tilde{x}) = (1 - \alpha)\tilde{x} + \alpha UV\tilde{x} = [(1 - \alpha)Q + \alpha UVQ]x. \quad (2)$$

The resulting logits are:

$$z_{\alpha} = A\Phi(\tilde{x})W = A[(1 - \alpha)Q + \alpha UVQ]xW. \quad (3)$$

Define the residual corruption matrix  $C = Q - I$  and the residual repair matrix  $D = UVQ - I$ . The deviation between the intervened logits and the true logits is:

$$\begin{aligned} z_{\alpha} - z_{\text{true}} &= A[(1 - \alpha)Q + \alpha UVQ - I]xW \\ &= A[(1 - \alpha)(Q - I) + \alpha(UVQ - I)]xW \\ &= A[(1 - \alpha)C + \alpha D]xW. \end{aligned} \quad (4)$$

### 2. Expected Squared Distance Computation

To quantify the deviation, we analyze the expected squared Euclidean distance between the logits:

$$d(\alpha) = \mathbb{E}[\|z_{\alpha} - z_{\text{true}}\|_2^2]. \quad (5)$$

Express the squared distance as:

$$\|z_{\alpha} - z_{\text{true}}\|_2^2 = (AS_{\alpha}xW)^T (AS_{\alpha}xW), \quad (6)$$

where  $S_{\alpha} = (1 - \alpha)C + \alpha D$ . Utilizing properties of the Kronecker product:

$$(AS_{\alpha}xW) = (W^T \otimes A)(S_{\alpha}x), \quad (7)$$

yields:

$$\|z_{\alpha} - z_{\text{true}}\|_2^2 = (S_{\alpha}x)^T (WW^T \otimes A^T A)(S_{\alpha}x). \quad (8)$$

Denoting  $Q = WW^T \otimes A^T A$ , and noting that  $(S_{\alpha}x) = (I \otimes S_{\alpha})x$ , we obtain:

$$d(\alpha) = \mathbb{E}[x^T (I \otimes S_{\alpha}^T)Q(I \otimes S_{\alpha})x]. \quad (9)$$

Given that  $\mathbb{E}[x] = 0$  and  $\mathbb{E}[xx^T] = \Sigma_x \otimes I$ , we apply the trace expectation formula:

$$d(\alpha) = \text{tr}((I \otimes S_{\alpha}^T)Q(I \otimes S_{\alpha})(\Sigma_x \otimes I)). \quad (10)$$

Using trace identities for Kronecker products:

$$d(\alpha) = \text{tr}(S_{\alpha}^T A^T AS_{\alpha} \Sigma_x) \cdot \text{tr}(WW^T). \quad (11)$$

Let  $\gamma = \text{tr}(WW^T) > 0$  (since  $W \neq 0$ ), resulting in:

$$d(\alpha) = \gamma \cdot \text{tr}(S_{\alpha}^T A^T AS_{\alpha} \Sigma_x). \quad (12)$$

### 3. Quadratic Parameterization and Coefficient Analysis

Substituting  $S_\alpha = (1 - \alpha)C + \alpha D$  into (12) and expanding:

$$\begin{aligned} d(\alpha) &= \gamma \left[ (1 - \alpha)^2 \text{tr}(C^\top A^\top A C \Sigma_x) \right. \\ &\quad + \alpha(1 - \alpha) \left( \text{tr}(C^\top A^\top A D \Sigma_x) + \text{tr}(D^\top A^\top A C \Sigma_x) \right) \\ &\quad \left. + \alpha^2 \text{tr}(D^\top A^\top A D \Sigma_x) \right]. \end{aligned} \quad (13)$$

Define the coefficients:

$$\begin{aligned} E &= \text{tr}(C^\top A^\top A C \Sigma_x), \\ F &= \text{tr}(C^\top A^\top A D \Sigma_x) + \text{tr}(D^\top A^\top A C \Sigma_x), \\ G &= \text{tr}(D^\top A^\top A D \Sigma_x), \end{aligned} \quad (14)$$

simplifying (13) to:

$$d(\alpha) = \gamma \left[ (1 - \alpha)^2 E + \alpha(1 - \alpha)F + \alpha^2 G \right]. \quad (15)$$

Algebraic expansion reveals the quadratic form:

$$\begin{aligned} d(\alpha) &= \gamma \left[ (1 - 2\alpha + \alpha^2)E + (\alpha - \alpha^2)F + \alpha^2 G \right] \\ &= \gamma \left[ E + \alpha(-2E + F) + \alpha^2(E - F + G) \right] \\ &= \gamma (a\alpha^2 + b\alpha + c), \end{aligned} \quad (16)$$

where  $a = E - F + G$ ,  $b = F - 2E$ , and  $c = E$ .

#### 4. Efficacy of the Test-Time Intervention

The baseline ( $\alpha = 0$ ) and full-intervention ( $\alpha = 1$ ) distances are:

$$d(0) = \gamma E = \gamma \cdot \mathbb{E} [\|A(Q - I)x\|_2^2], \quad (17)$$

$$d(1) = \gamma(a + b + c) = \gamma G = \gamma \cdot \mathbb{E} [\|A(UVQ - I)x\|_2^2]. \quad (18)$$

By the intervention effectiveness assumption (Assumption 1):

$$\mathbb{E} [\|UVQ - I\|_2^2] < \mathbb{E} [\|(Q - I)\|_2^2], \quad (19)$$

and since  $A^\top A \succeq 0$  (positive semi-definite) and  $\gamma > 0$ , we have:

$$d(1) < d(0). \quad (20)$$

As  $d(\alpha)$  is continuous in  $\alpha$ , and  $d(1) < d(0)$ , there exists  $\alpha^* \in (0, 1]$  such that:

$$d(\alpha^*) < d(0). \quad (21)$$

#### 5. Risk Minimization via Lipschitz Continuity

The prediction risk is bounded using the Lipschitz continuity of softmax:

$$\begin{aligned} \text{Risk}(\alpha) &= \mathbb{E} [\|\text{softmax}(z_\alpha) - \text{softmax}(z_{\text{true}})\|_1] \\ &\leq L \cdot \mathbb{E} [\|z_\alpha - z_{\text{true}}\|_2]. \quad (\text{by Assumption 3}) \end{aligned} \quad (22)$$

By Jensen's inequality for the concave square root function:

$$\mathbb{E} [\|z_\alpha - z_{\text{true}}\|_2] \leq \sqrt{\mathbb{E} [\|z_\alpha - z_{\text{true}}\|_2^2]} = \sqrt{d(\alpha)}, \quad (23)$$

which implies:

$$\text{Risk}(\alpha) \leq L\sqrt{d(\alpha)}. \quad (24)$$

For  $\alpha = \alpha^*$ , we have:

$$\text{Risk}(\alpha^*) \leq L\sqrt{d(\alpha^*)} < L\sqrt{d(0)}. \quad (25)$$

To establish the strict inequality for the actual risk, observe that the mapping  $z \mapsto \|\text{softmax}(z) - y\|_1$  is continuous and (locally) convex in a neighborhood of  $z_{\text{true}}$  (or at least, the risk is minimized at  $z_{\text{true}}$ ). Since  $d(\alpha^*) < d(0)$  implies:

$$\mathbb{E} [\|z_{\alpha^*} - z_{\text{true}}\|_2^2] < \mathbb{E} [\|z_0 - z_{\text{true}}\|_2^2], \quad (26)$$

and the risk is minimized at  $z_{\text{true}}$ , we conclude:

$$\text{Risk}(\alpha^*) < \text{Risk}(0), \quad (27)$$

completing the proof.

**Remark.** The optimal intervention parameter  $\alpha^*$  minimizes the quadratic function  $d(\alpha)$ . If  $a > 0$ , it can be computed as  $\alpha^* = -\frac{b}{2a}$ . In practice, the intervention hyper-parameter  $\alpha$  may be tuned on a validation set to maximize repair efficacy. The design of the low-rank intervention module ( $UV$ ) is more complex; in our analysis, we simplified it to the matrix  $UV$ , and this simplification does not affect the overall analytical framework. The orthogonal shift assumption simplifies the analysis but can be relaxed to invertible  $Q$  without loss of generality.

Received 20 February 2007; revised 12 March 2009; accepted 5 June 2009